Advanced numerical simulation based on a non-local micromorphic model for metal forming processes

Evangelia Diamantopoulou[1,a], Carl Labergere[1], Houssem Badreddine[1] and Khemais Saanouni[1]

[1]*University of Technology of Troyes, ICD/LASMIS UMR-CNRS 6281, 12 rue Marie Curie CS 42060 Troyes Cedex, France*

Abstract. An advanced numerical methodology is developed for metal forming simulation based on thermodynamically-consistent nonlocal constitutive equations accounting for various fully coupled mechanical phenomena under finite strain in the framework of micromorphic continua. The numerical implementation into ABAQUS/Explicit is made for 2D quadrangular elements thanks to the VUEL users' subroutine. Simple examples with presence of a damaged area are made in order to show the ability of the proposed methodology to describe the independence of the solution from the space discretization.

1 Introduction

Nowadays, the fully local constitutive equations have been well established to model the induced material softening behaviour due to thermal, damage and other microstructure-dependent phenomena. However, the solutions of the fully local constitutive equations are highly sensitive to the space and time discretization. The mechanics of generalized continua makes possible the straightforward introduction of the characteristic lengths into the constitutive equations of materials with microstructure in order to overcome this drawback [7]. Among others, the most recent and comprehensive review of these generalized continua and their use to solve various problems in mechanics of solids and fluids is found in the recent books and publications ([22,23], [24], [2], [7]). The micromorphic theory was proposed simultaneously by (Eringen and Suhubi, 1964[25]; Mindlin, 1964[26]). It consists of introducing a general non-compatible full field of micro-deformation as an extra degree of freedom, in addition to the classical displacement field. The micromorphic approach can, in fact, be applied to any macroscopic quantity in order to introduce a character length scale in the original classical continuum model in a systematic way, as presented by ([7], [8]). From the comparison between nonlocal and micromorphic theories, Forest and Aifantis [27] concluded that when the micromorphic variable remains as close as possible to the plastic strain, the micromorphic model reduces to the strain gradient theory.

The main goal of this paper is to show the efficiency of the formulated fully coupled nonlocal micromorphic constitutive equations in getting really mesh independent solutions even with high values of the ductile damage. The concept of internal lengths, that have to be experimentally determined from accurate measurements by using advanced methods, is introduced.

The introduction of the new balance equations in the nonlocal model with the effect of the ductile damage demands the construction of an element based on the assumed strain method combined with the Hu-Washizu variational form. The standard B matrix obtained from the displacement field analytically and including the hourglass control part, is projected to eliminate volumetric and shear locking phenomena. An air bending test of a DP1000 dual phase steel sheet is performed to validate and to show the mesh independent solution predicted by the micromorphic nonlocal model. This kind of nonlocal elastoplastic constitutive equations with damage can be later used for the numerical simulation of various sheet and bulk metal forming processes.

2 Theoretical aspects

2.1 The generalized principle of virtual power

The virtual power of internal forces of the classical local continuum is extended to the micromorphic continuum by using the virtual micromorphic damage ([2, 7]):

$$P_{\text{int}}\left(\vec{u}^*,\breve{d}^*\right)=-\int_V\left(\underline{\sigma}:\left(\vec{\nabla}\dot{\vec{u}}\right)^*+\breve{Y}\dot{\breve{d}}^*+\vec{\breve{Y}}\cdot\vec{\nabla}\dot{\breve{d}}^*\right)dV \qquad (1)$$

where, $\underline{\sigma}$ is the Cauchy stress tensor, the scale $\breve{Y}$ and vector $\vec{\breve{Y}}$ are the stress-like variables with respect to micromorphic damage $\breve{d}$ and its first gradient $\vec{\nabla}\breve{d}$.
Similarly, the virtual power of external forces can be also extended with the simple and generalized body forces $\vec{f}^u$, $f^{\breve{d}}$ and $\vec{f}^{g\breve{d}}$, and contact forces $\vec{F}^u$ and $F^{\breve{d}}$:

[a] evangelia.diamantopoulou@utt.fr

$$P_{ext}\left(\vec{u}^*,\breve{d}^*\right)=\rho\int_V\left(\vec{f}^u\cdot\dot{\vec{u}}^*+f^{\breve{d}}\dot{\breve{d}}^*+\vec{f}^{g\breve{d}}\cdot\vec{\nabla}\dot{\breve{d}}^*\right)dV+\int_\Gamma\left(\vec{F}^u\cdot\dot{\vec{u}}^*+F^{\breve{d}}\dot{\breve{d}}^*\right)dS \quad (2)$$

The virtual power of the inertia forces are enhanced by the micromorphic phenomena:

$$P_a\left(\vec{u}^*,\breve{d}^*\right)=\rho\int_V\left(\ddot{\vec{u}}\cdot\dot{\vec{u}}^*+\zeta_{\breve{d}}\ddot{\breve{d}}\dot{\breve{d}}^*\right)dV \quad (3)$$

where, $\zeta_{\breve{d}}$ is a scale factor which maps the local density to the micromorphic level.

The generalized virtual power enhanced with the micromorphic damage takes the following form for any given kinematically admissible fields:

$$P_{\text{int}}+P_{ext}=P_a \qquad \forall\vec{u}^*,\breve{d}^*\ K.A. \quad (4)$$

Substitute Eq. (1) to Eq. (3) into the generalized form of virtual power Eq. (4), and by using the divergence theorem to transform the volume integrals, leads to the two momentum equations:

$$\begin{cases}\vec{\nabla}\cdot\underline{\sigma}+\rho\vec{f}^u=\rho\ddot{\vec{u}} & in\ \Omega\\ \underline{\sigma}\cdot\vec{n}=\vec{F}^u & on\ \Gamma\end{cases} \quad (5a)$$

$$\begin{cases}\left(\vec{\nabla}\cdot\vec{\breve{Y}}+\breve{Y}\right)+\rho\left(f^{\breve{d}}-\vec{\nabla}\cdot\vec{f}^{g\breve{d}}\right)=\rho\zeta_{\breve{d}}\ddot{\breve{d}} & in\ \Omega\\ \left(\vec{\breve{Y}}-\rho\vec{f}^{g\breve{d}}\right)\cdot\vec{n}=F^{\breve{d}} & on\ \Gamma\end{cases} \quad (5b)$$

The two partial differential equations are the strong forms with respect to displacement and micromorphic damage with Initial Boundary Value Problem (IBVP). And the stress-like variables $\underline{\sigma}$, $\breve{Y}$ and $\vec{\breve{Y}}$ will be defined by the state relations developed under the framework of thermodynamic irreversible processes.

2.2 State relations

In this section, a specific state potential as well as yield function and dissipation potential are constructed for an isothermal isotropic elastoplasticity fully coupled with isotropic local damage, isotropic and kinematic hardening and isotropic micromorphic damage. The damaged state variables are applied to the local state variables according to the assumption of the equivalence of total energy developed in (see [12-15], [16], [17], [18], [19], [7], [21, 22]). And for simplification, we also postulate that only the local damage is coupled with the micromorphic damage. With these assumptions, a quadratic the Helmholtz free energy can be expressed as:

$$\rho\psi=\frac{1}{2}(1-d)\left(\underline{\varepsilon}^e:\underline{\underline{\Lambda}}:\underline{\varepsilon}^e+\frac{2}{3}C\underline{\alpha}:\underline{\alpha}\right)+\frac{1}{2}\left(\left(1-d^\gamma\right)Qr^2+\breve{H}\left(d-\breve{d}\right)^2+\breve{H}^g\vec{\nabla}\breve{d}\cdot\vec{\nabla}\breve{d}\right) \quad (6)$$

where $\underline{\underline{\Lambda}}=\lambda_e\underline{1}\otimes\underline{1}+2\mu_e\underline{\underline{1}}$ is the fourth-rank elastic tensor expressed with the classical Lame's parameters. C and Q are the macro modules of kinematic and isotropic hardening respectively. $\breve{H}$ is the micromorphic module with respect to local damage and micromorphic damage. $\breve{H}^g$ is the micromorphic module related to the gradient of micromorphic damage.

The local and nonlocal stress-like variables are derived in the following forms:

$$\underline{\sigma}=\rho\frac{\partial\psi}{\partial\underline{\varepsilon}^e}=(1-d)\underline{\underline{\Lambda}}:\underline{\varepsilon}^e=(1-d)\left(\lambda_e tr\left(\underline{\varepsilon}^e\right)\underline{1}+2\mu_e\underline{\varepsilon}^e\right) \quad (7)$$

$$\underline{X}=\rho\frac{\partial\psi}{\partial\underline{\alpha}}=\frac{2}{3}(1-d)C\underline{\alpha} \quad (8)$$

$$R=\rho\frac{\partial\psi}{\partial r}=\left(1-d^\gamma\right)Qr \quad (9)$$

$$Y=-\rho\frac{\partial\psi}{\partial d}=\frac{1}{2}\left(\underline{\varepsilon}^e:\underline{\underline{\Lambda}}:\underline{\varepsilon}^e+f_h\frac{2}{3}C\underline{\alpha}:\underline{\alpha}+f_h(\gamma/2)d^{\gamma-1}Qr^2\right)-f_h\breve{H}\left(d-\breve{d}\right)=Y^e+f_h(Y^\alpha+Y^r+\breve{Y}) \quad (10)$$

$$\breve{Y}=\rho\frac{\partial\psi}{\partial\breve{d}}=-\breve{H}\left(d-\breve{d}\right) \quad (11)$$

$$\vec{\breve{Y}}=\rho\frac{\partial\psi}{\partial\vec{\nabla}\breve{d}}=\breve{H}^g\vec{\nabla}\breve{d} \quad (12)$$

In Eq. (10) γ is the parameter governing the effect of the damage on the isotropic hardening and f_h a simple function equal to 1 if the hydrostatic part of the stress is positive, else it is equal to 0.

The energy density release rate given by state relation with respect to damage in Eq. (10) can be decomposed into local part and coupled nonlocal part:

$$\begin{cases}Y=Y_{loc}+Y_{nloc}\\ Y_{loc}=\frac{1}{2}\left(\underline{\varepsilon}^e:\underline{\underline{\Lambda}}:\underline{\varepsilon}^e+\frac{2}{3}C\underline{\alpha}:\underline{\alpha}+\gamma d^{\gamma-1}Qr^2\right)\\ Y_{nloc}=\breve{Y}=-\breve{H}\left(d-\breve{d}\right)\end{cases} \quad (13)$$

2.3 Evolution equations

Since there's no dissipation from micromorphic damage, to account for the damage effects, we limit ourselves to the isotropic plasticity for simplicity. The von Mises yield function and dissipation potentials used in ([7], [12-14], [16], [17], [18], [19]) are used:

$$f\left(\underline{\sigma},\underline{X},R;d\right)=\frac{\left\|\underline{\sigma}-\underline{X}\right\|}{\sqrt{1-d}}-\frac{R}{\sqrt{1-d^\gamma}}-\sigma_y\le 0 \quad (14)$$

$$F\left(\underline{\sigma},\underline{X},R,d\right)=f+\frac{3}{4}\frac{a\underline{X}:\underline{X}}{C(1-d)}+\frac{1}{2}\frac{bR^2}{Q\left(1-d^\gamma\right)}+\frac{S}{(s+1)(1-d)^\beta}\left\langle\frac{Y-Y_0}{S}\right\rangle^{(s+1)} \quad (15)$$

where, $\|\underline{\sigma}-\underline{X}\|=\sqrt{(3/2)(\underline{\sigma}^{dev}-\underline{X}):(\underline{\sigma}^{dev}-\underline{X})}$ defines the well-known von Mises equivalent stress and $\underline{\sigma}^{dev}$ is its deviatoric part of the stress tensor. The parameters α and b reflect the nonlinear property of the kinematic and isotropic hardening respectively and S, s and β characterize the nonlinear evolution of the ductile damage.

Clearly, the yield function and plastic potential are identical to the local theory. However, the indirect contribution of the micromorphic state variables is introduced from the state relations. Applying the generalized normality rule to the above defined local yield function and dissipation potential lead to the following evolution equations:

$$\underline{\dot{D}}^{p}=\dot{\lambda}\frac{\partial F}{\partial\underline{\sigma}}=\dot{\lambda}\underline{\tilde{n}}=\dot{\lambda}\frac{\underline{n}}{\sqrt{1-d}} \tag{16}$$

$$\underline{\dot{\alpha}}=-\dot{\lambda}\frac{\partial F}{\partial\underline{X}}=\dot{\lambda}\left(\frac{\underline{n}}{\sqrt{1-d}}-a\underline{\alpha}\right) \tag{17}$$

$$\dot{r}=-\dot{\lambda}\frac{\partial F}{\partial R}=\dot{\lambda}\left(\frac{1}{\sqrt{1-d^{\gamma}}}-br\right) \tag{18}$$

$$\dot{d}=\dot{\lambda}\frac{\partial F}{\partial Y}=\frac{\dot{\lambda}}{(1-d)^{\beta}}\langle\frac{Y-Y_0}{S}\rangle^{s} \tag{19}$$

where $\underline{n}=3(\underline{\sigma}^{dev}-\underline{X})/2\,\|\underline{\sigma}-\underline{X}\|$ is the outside normal to the yield surface in the stress space and $\dot{\lambda}$ is the plastic multiplier.

2.4 Transformation of the micromorphic balance equations

Considering the generalized balance equation of micromorphic momentum Eq. (5b), it can be easily expressed in strain-like variables space by using micromorphic state relations Eq. (11) and Eq. (12):

$$\begin{cases}\left(\breve{H}^{g}Lap\left(\breve{d}\right)-\breve{H}\left(d-\breve{d}\right)\right)+\rho\left(f^{\breve{d}}-\vec{\nabla}\cdot\vec{f}^{g\breve{d}}\right)=\rho\zeta_{D}\ddot{\breve{d}} & in\ \Omega\\ \left(\breve{H}^{g}\left(\vec{\nabla}\breve{d}\right)-\rho\vec{f}^{g\breve{d}}\right)\cdot\vec{n}=F^{\breve{d}} & on\ \Gamma\end{cases} \tag{20}$$

By neglecting the micromorphic body forces , i.e. $f^{\breve{d}}=0$, $\vec{f}^{g\breve{d}}=0$ and $F^{\breve{d}}=0$, the above equation can take the following form:

$$\begin{cases}l_{\breve{d}}^{2}Lap\left(\breve{d}\right)-\left(d-\breve{d}\right)=\rho\dfrac{\zeta_{\breve{d}}}{\breve{H}}\ddot{\breve{d}} & in\ \Omega\\ \left(\breve{H}^{g}\left(\vec{\nabla}\breve{d}\right)\right)\cdot\vec{n}=0 & on\ \Gamma\end{cases} \tag{21}$$

where, $l_{\breve{d}}$ is the intrinsic internal length scale parameter relative to the micromorphic damage defined as the ratio of the micromorphic moduli:

$$l_{\breve{d}}^{2}=\frac{\breve{H}^{g}}{\breve{H}} \tag{22}$$

The Eq. (21) is used as a strong form from which the associated weak form will be deduced in order to solve the fully coupled IBVP.

3 Internal lengths

The development of an 'advanced' modelling of multiphysic thermomechanical coupling in the framework of the generalized continuum mechanics (micromorphic theory) is proposed in order to introduce the concept of internal lengths that are representative of the materials microstructures while accounting for the various initial and induced anisotropies under large deformations. These internal lengths have to be experimentally determined from accurate measurements of highly localized displacement/strain (or velocity/strain rate) fields by using advanced methods to measure the kinematic fields at the relevant scales. For that, the electronic speckle pattern interferometry (ESPI) method will be used.

We seek to locally measure the displacement and velocity fields in order to access to the local strain/strain rate fields inside the localized zones. An example of a localization pattern obtained with the ESPI technique on a 460 steel sheet is shown in Figure 1 [6]. The tensile direction is horizontal and the interference fringes due to the displacement field are shown in the left where each grey level corresponds to 2.8 nm and the total relative displacement is about 3 µm. The corresponding strain rate field (tensile component) extracted with the geometrical model is shown in the right. The widths B1 and B2 of the localization bands are obtained directly from the experimental measure. These experimental measurements will provide inputs for the advanced micromorphic constitutive equations and mainly to determine the internal lengths related to the targeted micromorphic phenomena [5].

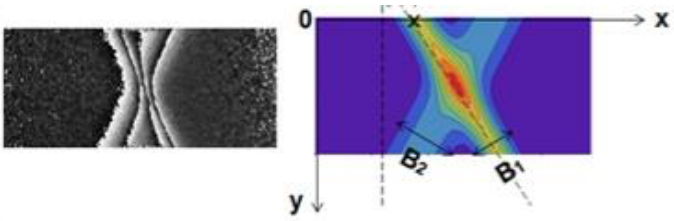

Figure 1. Illustration of the parameters, the image on the left is a fringe pattern and that on the right is the corresponding strain rate map obtained [6].

A purely geometric (or kinematic) model used to describe the strain rate pattern and extract global parameters. It is independent of the constitutive

behaviour of the material. The strain rate distribution in each band is depicted by a linear combination of a Gaussian and a Lorentzian function:

$$\dot{\varepsilon}_{xx}(x,y) = \dot{\varepsilon}_1^{\max}(\eta_1 G_1 + (1-\eta_1)L_1) + \dot{\varepsilon}_2^{\max}(\eta_2 G_2 + (1-\eta_2)L_2) \quad (23)$$

where $\dot{\varepsilon}_i^{\max}$ is the maximum strain rate, G_i is a Gaussian function, L_i is a Lorentzian function, η_i and $1-\eta_i$ are the weights of the Gaussian and the Lorentzian functions respectively ($i \in \{1, 2\}$).

The Gaussian and Lorentzian functions are defined as following:

$$G(a,b,B,x,y)\exp(-\pi(\frac{x-ay-b}{B})^2)$$
$$L(a,b,B,x,y) = \frac{1}{1+(\pi\frac{x-ay-b}{B})^2} \quad (24)$$

with:

- a , the inclination of the band with respect to the transverse direction.
- b , the location of the band.
- B , the integral width of the band.

In all cases of the present study, the specimens failed in the same direction, along the band that was oriented almost perpendicular to the rolling direction or along band 1 as illustrated in **Fig.1**. Thereby to simplify the explications, this band will be called dominant band and the other one disappearing band, and the superscript "dom" and "dis" will be used to indicate them.

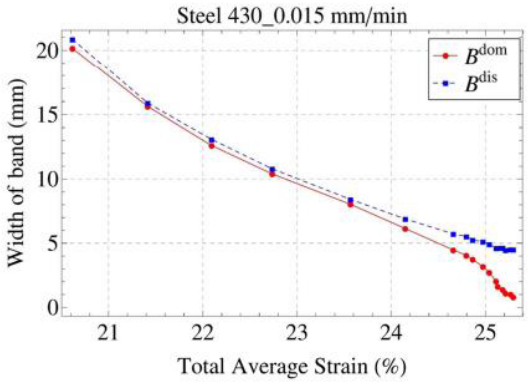

Figure 2. Evolutions of the localization band characters vs total average strain (or time) with different tensile speed. Maximum strain rate of the bands vs total average strain, bandwidth vs total average strain [6].

For the identification of the internal lengths, an effort is under progress. According to the analytical-experimental study described above, an experimental-numerical study is evolving in order to determine the values of $\breve{H}$ and $\breve{H}^g$ and verify the characteristic length for each material and mesh size in total agreement with the experiments and the information extracted by **Fig.2** (bandwidths, total average strain, estimated error between numerical and experimental strain rate etc).

Let us note here, that the above study concerns a 460 (X8Cr17) steel specimen.

For this paper and the air bending application presented in section 5, a DP1000 dual phase sheet is used. The internal length for this type of material is determined empirically and fixed at $\sim 0.2mm$ by following the rule that **M**esh **s**ize (**Ms**) $< l_d$.

4 Numerical aspects

From the numerical point of view, an advanced numerical procedure is presented. The finite element code that is used to implement the micromorphic model is developed in ABAQUS®. The numerical integration in mixed one/four quadrature(s) (or Gauss) point for all the coupled constitutive equations is necessary in order to compute the stress tensor and the overall stress-like internal variables which appear in the weak forms associated to the balance equations. For the time discretization of the equations of our behaviour model, the fully implicit (iterative) Euler scheme in combination with an asymptotic one applied to the hardening equations are used. The overall constitutive equations are then reduced to two nonlinear and strongly coupled algebraic equations (for the isotropic plasticity) with two unknowns: $\Delta\lambda$ and d_{n+1}. The elastic prediction-plastic correction method is then used together with the Newton-Raphson resolution scheme to solve the two equations. The behaviour model defined in the framework of the micromorphic continua is implemented into ABAAQUS/Explicit® thanks to the VUMAT user's subroutine.

The introduction of the new micromorphic balance equations in the behaviour model with nonlocal damage demands the construction of a special element based on a mixed variational form and having $\breve{d}$ as additional d.o.f. Fish and Belytschko (see [4]) proposed an extension of the Hu-Washizu weak form of the variational principle in nonlinear mechanics of solids. We consider two variational forms and introduce balance equation with the contribution of the micromorphic damage discretized on a domain **Ω**.

The weak form of the balance equations can be obtained thanks to the weighted residual method [4] in order to get:

$$\begin{cases} \int_\Omega \underline{\sigma}_a : \delta\underline{\varepsilon}_a d\Omega + \delta\int_\Omega \underline{\sigma}_a : \left(\vec{\nabla}^{sym}(\vec{u}) - \underline{\varepsilon}_a\right) d\Omega - \delta W_{ext} = 0 \\ \int_\Omega \left(\breve{d}\delta\breve{d} + \ell_d^2(\vec{\nabla}\breve{d}).(\vec{\nabla}\delta\breve{d})\right) d\Omega - \int_\Omega \left(d\delta\breve{d}\right) d\Omega = 0 \end{cases} \quad (25)$$

where δW_{ext} is the external forces virtual work, δ represents the classical variation operator, $\vec{u}$ is the displacement vector, $\underline{\sigma}$ the Cauchy stress tensor, $\underline{\varepsilon}_a$ the tensor of the assumed strains, $\underline{\sigma}_a$ the assumed stress tensor and $\underline{\nabla}^s(\vec{u})$ is the symmetric part of the displacement gradient. Simo and Hughes [9] suggested the construction of the projection of the velocity field's discretized gradient $\left[B^e_{n+1/2}\right]$. This new operator is chosen

in order to evaluate the assumed strain tensor $\left\{\varepsilon^a\right\}_{n+1}=\left[B^e_{n+½}\right]\left\{\dot{u}^e\right\}_{n+½}$ and to compute the associated assumed stress tensor $\left\{\sigma^a_{n+1}\right\}$ which is orthogonal to the difference between the symmetric part of the velocity gradient and the assumed strain tensor. This choice allows us to simplify the Hu-Washizu weak form as follows:

$$\begin{cases} \int_\Omega \underline{\sigma}_a : \delta\underline{\varepsilon}_a d\Omega - \delta W_{ext} = 0 \\ \int_\Omega \left(\breve{d}\delta\breve{d} + \ell_d^2(\vec{\nabla}\breve{d}).(\vec{\nabla}\delta\breve{d})\right)d\Omega - \int_\Omega \left(d\delta\breve{d}\right)d\Omega = 0 \end{cases} \quad (26)$$

The matrix $\left[B^e_{n+½}\right]$ is decomposed in two parts: $\left[B^0_{n+½}\right]$ for the tensile and shear modes that gives the stress tensor components in the centre of the element, and $\left[B^h_{n+½}\right](\xi,\eta)=\xi\left[B^\xi_{n+½}\right]+\eta\left[B^\eta_{n+½}\right]$ for the control of the hourglass modes for all the elements. Finally, the expression of the total strain tensor, according to the assumptions above, is written as follows:

$$\left\{\varepsilon^a\right\}_{n+1}=\left[B^e_{n+½}\right]\left\{\hat{u}^e\right\}_{n+½}=\underbrace{\left[B^0_{n+½}\right]\left\{u^e\right\}_{n+½}}_{\left\{D^0\right\}_{n+1}}+\underbrace{\left[B^h_{n+½}\right]\left\{u^e\right\}_{n+½}}_{\left\{D^h\right\}_{n+1}}$$
$$=\left\{\varepsilon^0\right\}_{n+1}+\left\{\varepsilon^h\right\}_{n+1} \quad (27)$$

Wang et al [1] proposed the construction of a quadrangular element to the field of the assumed strains in a 2D plane strain in order to control the shear and volumetric locking. The isoparametric shape functions for the 4-node quadrilateral can be written in terms of a set of orthogonal base vectors as:

$$N_i(\xi,\eta)=\frac{1}{4}\mathbf{s}+\frac{1}{4}\boldsymbol{\xi}\xi+\frac{1}{4}\boldsymbol{\eta}\eta+\frac{1}{4}\mathbf{h}\xi\eta \quad (28)$$

where (ξ,η) are the coordinates in the reference space with $\boldsymbol{\xi}^T=[-1,1,1,-1]$, $\boldsymbol{\eta}^T=[-1,-1,1,-1]$, $\mathbf{s}$ is the translation vector with $\mathbf{s}=[1,1,1,1]$ and $\mathbf{h}$ is the hourglass vector with $\mathbf{h}=[1,-1,1,-1]$.

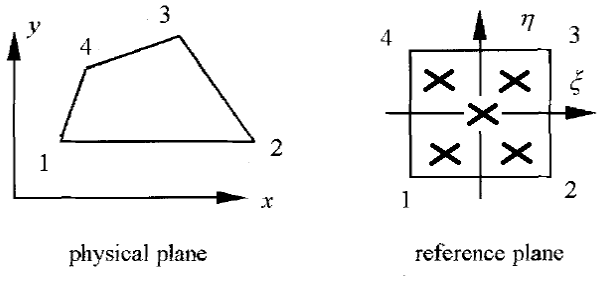

Figure 3. A 4-node quadrilateral element in physical and natural coordinate systems.

This element is used in our formulations by adding a new degree of freedom associated to the nonlocal damage. In order to ensure the objectivity of the model, corotational local system is built in the centre of the element using the shape functions defined in the reference space (ξ,η). The orientation of this corotational triad is governed by rotation tensor $\underline{Q}$ which is expressed under the following form:

$$[Q]=\begin{bmatrix} e_1^1 & e_1^2 \\ e_2^1 & e_2^2 \end{bmatrix},\ \vec{g}_1=\frac{\partial x}{\partial\xi}\vec{x}+\frac{\partial x}{\partial\eta}\vec{y},\ \vec{e}_1=\frac{\vec{g}_1}{\|\vec{g}_1\|},\ \vec{e}_2.\vec{e}_1=0,\ \|\vec{e}_2\|=1 \quad (26)$$

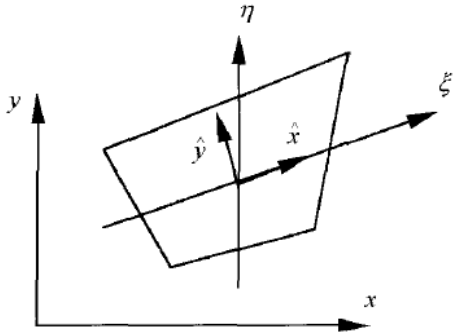

Figure 4. Corotational system definition of the Q4-URI element [1].

5 Numerical simulation of the air bending test

The air bending test was modelled in a 2D plane strain configuration. The sheet is discretized with the Q4 quadrangular element implemented in a VUEL ABAQUS/Explicit® subroutine.

The DP1000 steel material parameters have been determined by an inverse approach [11] based on the experimental results: *E=220.0 GPa, ν=0.3, σ_y=810.0 MPa, Q=3800.0 MPa, b=15.0, C=69500.0 MPa, a=240.0, S=12.0 MPa, s=1.2, β=1.0, Y_0=0.0, γ=4.0.*
3D measurement of strain conducted via Aramis-GOM system make to measure the strain distribution over the specimen and fracture strain, respectively.

5.1 Behaviour model with local damage

Initially, $\breve{H}=\breve{H}^g=0$ is chosen. Figure 5 shows the isovalues of the internal damage '*d*' for the three different mesh sizes. It is clear that the size of the localization zone depends on the mesh size.

For this case the results of damage mapped the at final fracture stage are obtained for different mesh sizes. This figure shows clearly that the mesh size affects not only localization zone but also the moment of the final fracture (i.e. global displacement when the damage of an element reaches the value $'d=1'$, namely U_{rupt}). The dependence of the localization band to the mesh size leads to different values of fracture displacement in such a manner that smallest mesh size allows the smallest fracture displacement. This ascertainment is confirmed through global force/displacement curves given in Figure 6.

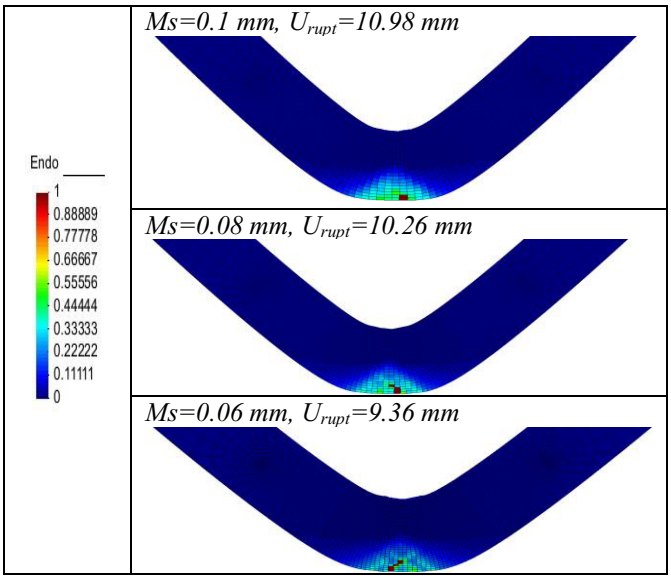

Figure 5. Damage isovalues of a ruptured DP1000 specimen in the framework of the local continua for different Ms.

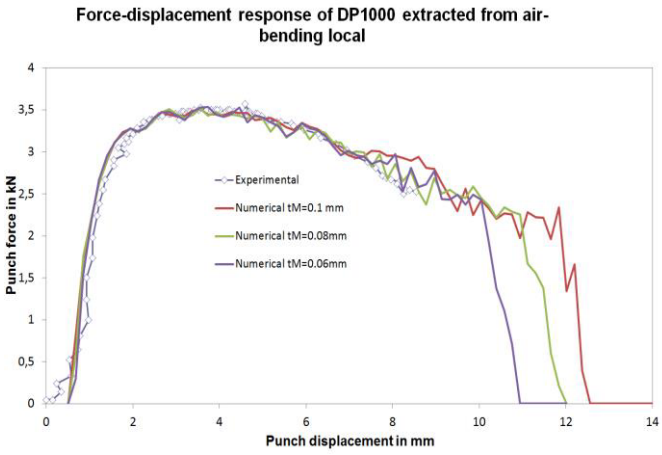

Figure 6. Experimental and numerical force-displacement curves of DP1000 for air-bending for the local model.

5.2 Behaviour model with nonlocal damage

The nonlocal formulation is taken into consideration by activating the contribution of the micromorphic damage variable $\breve{d}$ by setting $\breve{H} = 80N.mm^{-2}$, $\breve{H}^g = 3.6N$ and the internal length fixed at $\ell_{\breve{d}} = \sqrt{\breve{H}^g / \breve{H}} \approx 0.21mm$.

For this case, the results considering the damage are also obtained after testing on three different mesh sizes (Figure 7). We can see that the damage localization bandwidth becomes smoother than the local damage case (i.e. the damage gradient varies less than in the local case). The length of damage gradient appears virtually identical for the three mesh cases but the crack always propagates in final stage along a single row of elements. The regularization length makes it possible to calibrate the amount of damage dissipation that crosses a band and its influence is significant for the model's response. Unlike the local model, the force/displacement curve (see Figure 8) gives the same fracture displacement value at $U_{rupt} \approx 10.6mm$.

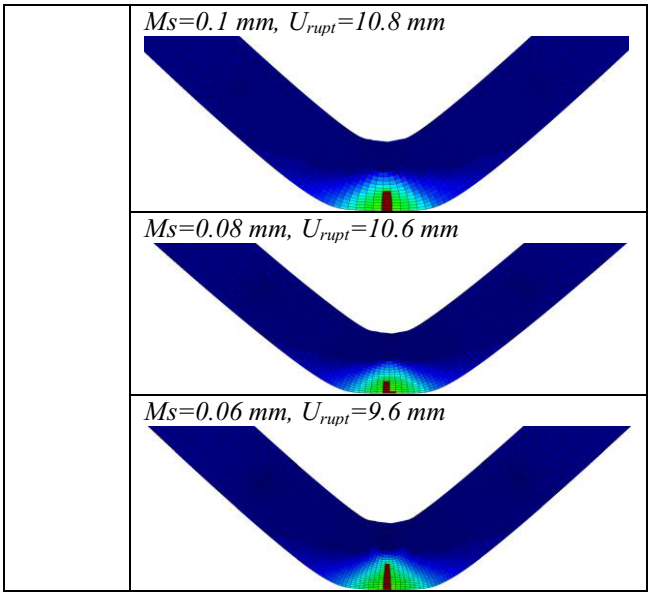

Figure 7. Damage isovalues of a ruptured DP1000 specimen in the framework of the nonlocal continua for different Ms

However, we observe a slight difference of the three results in the softening phase. This difference can be explained by the need to introduce a micromorphic variable associated with isotropic hardening in order to regularize this stage.

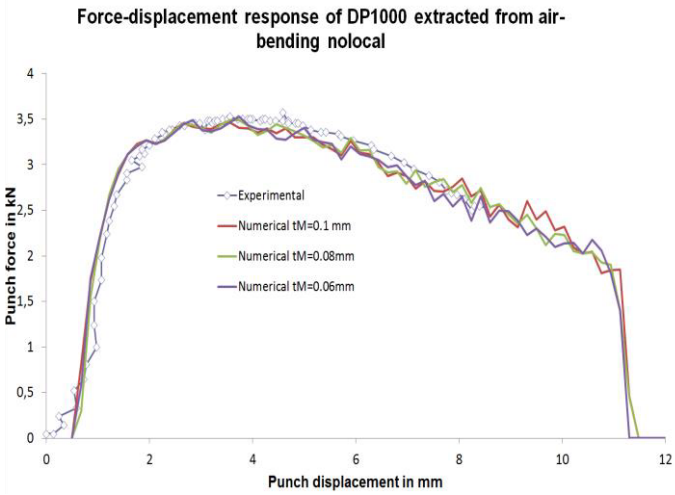

Figure 8. Experimental and numerical force-displacement curves of DP1000 for air-bending for the non-local model.

Acknowledgements

The authors acknowledge the financial support of the National Research Agency (ANR) as well as the contribution of their partners from LRM/UTC and CdM/Ecole des Mines in the project "MICROMORFING". Also Prof. M. François (UTT/LASMIS) and Ph.D C.Bao (UTT/LASMIS) are gratefully acknowledged for the experimental work.

References

1. J. Wang, J. Chen, M. Li, ACTA MECHANICA SNICA, Vol.20, No.6, December 2004.
2. K. Saanouni, ISTE, London, UK and John Wiley & Sons, Inc., Hoboken, NJ, USA, 2012.
3. M. Hamed, Ph.D. thesis, Université de Technologie de Troyes, 2012.
4. T. Belytscho, W.K. Liu, B. Moran, John Wiley & Sons Ltd, The Atrium, Southern Gate, Chichester, West Sussex, England , 2000.
5. C. Labergere, B. Guelorget, M. François, INTERNATIONAL JOURNAL OF SOLIDS AND STRUCTURES 51(S 23–24), pp. 3944–3961, 2014.
6. C. Bao, M. François, L. Le Joncour, Applied Mechanics and Materials Vol. 784, pp. 514-519, 2015.
7. K. Saanouni, M. Hamed, INTERNATIONAL JOURNAL OF SOLIDS AND STRUCTURES 50(S 14–15), pp. 2289–2309, 2013.
8. S. Forest, ASCE journal of engineering Mechanics, vol 135, pp. 177-131, 2009.
9. Simo J.C., Hughes T.J.R, Springer Verlag, New York, 1998.
10. C. Soyarslan, M. Malekipour Gharbi, A.E. Tekkaya, International Journal of Solids and Structures 49 (2012), pp. 1608–49 (13):1608-1626, 2012.
11. M. Gharbi, C. Labergere**,** H. Badreddine, C. Soyarslan, A. Weinrich, M. Hermes., S. Chatti, H. Sulaiman, K. Saanouni , A.E. Tekkaya., 10th International conference on technology of plasticity, pp. 25-30, September 2011.
12. Saanouni K, Forster C, Hatira FB, International Journal of Damage Mechanics 3 (2):140-169, 1994.
13. Saanouni K, Nesnas K, Hammi Y, International Journal of Damage Mechanics 9 (3):196-240, 2000.
14. Saanouni K, Cherouat A, Hammi Y, Revue européenne des éléments finis 2-3-4:327-351, 2001.
15. Saanouni K, Badreddine H, Ajmal M, Journal of engineering materials and technology 130 (2):02102201-02102211, 2008.
16. Saanouni K, Hammi Y, Elsevier, New York, 2000
17. Saanouni K, Chaboche J, Numerical and Computational Methods in Comprehensive Structural Integrity 3, 2003
18. Labergère C, Rassineux AA, Saanouni KK, International journal of material forming 4 (3):317-328, 2011
19. Issa M, Labergère C, Saanouni K, Rassineux, CIRP Journal of Manufacturing Science and Technology 5 (3):175-195, 2012
20. Badreddine H, Saanouni K, Dogui A, International Journal of Plasticity 26 (11):1541-1575, 2010.
21. Badreddine H, Saanouni K, Nguyen TD, International Journal of Solids and Structures 63:11-31, 2015.
22. Eringen AC, *Microcontinuum field theories: I,* Foundations and Solids. Springer Verlag, New York, 1999.
23. Eringen AC, *Nonlocal continuum field theories,* Springer Science & Business Media, 2002.
24. Forest S, *Milieux continus généralisés et matériaux hétérogènes,* Presses des MINES, 2006.
25. Eringen AC, Suhubi ES, International Journal of Engineering Science 2 (2):189-203, 1964.
26. 7. Mindlin RD, Arch Rational Mech Anal 16 (1):51-78, 1964.
27. Forest S, Aifantis EC, International Journal of Solids and Structures 47 (25–26):3367-3376, 2010.